Entropic lattice pseudo-potentials for multiphase flow simulations at high Weber and Reynolds numbers

A. Montessori,[1] P. Prestininzi,[1] M. La Rocca,[1] and S. Succi[2,3]
[1)] *University of "Roma Tre", Department of Engineering, Via Vito Volterra 62, 00146 Rome, Italy*[a)]
[2)] *Istituto per le Applicazioni del Calcolo, CNR Via dei Taurini 19, 00185 Rome - Italy*
[3)] *John A. Paulson School of Engineering and Applied Sciences, Harvard University, 29 Oxford Street, Cambridge, MA 02138, USA*

(Dated: 8 June 2022)

We present an entropic version of the lattice Boltzmann pseudo-potential approach for the simulation of multiphase flows. The method is shown to correctly simulate the dynamics of impinging droplets on hydrophobic surfaces and head-on and grazing collisions between droplets, at Weber and Reynolds number regimes not accessible to previous pseudo-potential methods at comparable resolution.

Keywords: LBM, entropic Lattice Boltzmann, multiphase flows, droplet dynamics, pseudo-potential lattice Boltmzann

https://aip.scitation.org/doi/abs/10.1063/1.5001253

I. INTRODUCTION

A deeper understanding of the physics of fluid-fluid and fluid-solid interfaces levels is paramount to the study of many natural and industrial processes, from rain dynamics to surface coatings and tissue manufacturing, to name but a few[1–3].

The complexity involved by the dynamics of the fluid interface makes such problems very hard to investigate, both analytically and numerically. From the experimental point of view, the complex phenomena which govern the dynamics of micro-droplets may become inaccessible to experiments[4], due to the technical difficulties of tracking the flow field at such small spatial scales. In addition, the typical Weber and Reynolds numbers involved in many realistic problems, such as surface droplet spreading, high-speed droplet impacts and spray-like break-up, are usually very high, thus implying extremely complex free surface deformations and internal flow circulations, which need to be accurately tracked to gain a solid understanding of these phenomena (see[5] for a thorough review of droplet break up phenomena). For these reasons, the development of robust and accurate computational models for complex interfacial dynamics, makes a subject of intense research[6,7].

In the last two decades, lattice kinetic theory has captured major attention for the simulation of a broad range of complex flows, from fluid turbulence to complex non equilibrium flows in complex media[8–11]. In particular, the lattice Boltzmann method (LB) has attracted significant attention, due to the possibility of simulating (non-ideal) multiphase and multicomponent flows within a simple and efficient computational framework[12,13]. Among others, the pseudo-potential approach has emerged as one of the most popular options within the LB community, mainly on account of its conceptual simplicity and computational flexibility. Namely, pseudopotential approaches for multiphase and multicomponent flows are easy to implement not requiring any ad hoc tracking of the fluid-fluid interfaces, as in VOF or level set methods as well as the computation of local values of the Kortwegg tensor (like in free energy models for multiphase flows) which require the discretization of gradients an Lapacians of the density field. Nevertheless, the original formulation of the pseudo-potential

[a)] Electronic mail: andrea.montessori@uniroma3.it

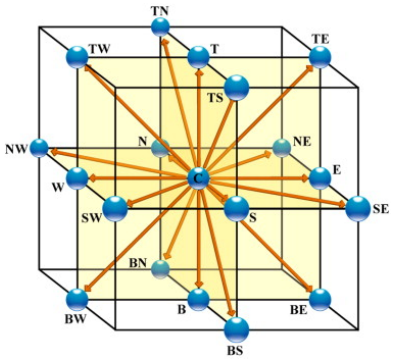

FIG. 1. (a) Sketch of the D3Q19 with nineteen discrete velocities in three dimensional space.

approach, due to Shan and Chen (SC)[12], suffers from several drawbacks, particularly the limited range of stable density ratios and a limited capability of dealing with high velocity flows required to access high Weber and high Reynolds numbers[14–16]. These limitations do not prevent the pseudo-potential approach from simulating a broad class of soft matter systems, like emulsions and glassy flows[17–19], featuring Reynolds numbers and density ratios accessible to the standard Shan-Chen approach. However, for many other problems characterised by high-speed and low-surface tension, i.e. high Reynolds and Weber numbers, appear to be beyond reach for the current pseudo-potential approach.

Recently the entropic LB, due to[20], has been extended to cover a large number of complex flow phenomena[15,21–23]. The essence of the entropic approach is to let the fluid viscosity adapt to sharp changes of the fluid structure in order to fulfil a local form of the second principle (H-theorem). This feature has been largely documented for the case of low-viscous (high-Reynolds) number flows[21], but only recently discussed in the framework of multiphase flows[15].

In this paper, we propose an entropic[20,24] pseudo-potential approach with variable vapour-liquid viscosity ratio, which allows to simulate droplet phenomena at Reynolds and Weber numbers above 10^3 and 10^2 respectively.
We then present several applications of the entropic pseudo-potential approach namely, impact of droplets with hydrophobic walls and head-on and off-axis collisions between droplets.

II. METHOD

The lattice Boltzmann equation with entropic relaxation[20,25] reads as follows:

$$f_i(\mathbf{x}+\mathbf{c}_i\Delta t, t+\Delta t) = f_i(\mathbf{x},t) - \omega(f_i - f_i^{eq}(\rho,\mathbf{u})) + S_i \tag{1}$$

where, $f_i(\mathbf{x},t)$ is the discrete distribution function providing the probability of finding a particle at lattice site $\mathbf{x}$ at time t with discrete velocity $\mathbf{c}_i$, being $i = 0,\ldots,b$ the number of lattice directions. In this work a three-dimensional 19 speed lattice (D3Q19) has been employed, fig. 1. The discrete local equilibrium $f_i^{eq}(\rho,\mathbf{u})$ minimizes the entropy function $H(f) = \sum_i f_i ln(f_i/w_i)$[26], where w_i is a set of positive weights associated to the lattice directions. In the above, ρ and $\mathbf{u}$ are the zeroth and first order statistical moments of the discrete set of distribution functions representing, respectively, the density $\rho = \sum_i f_i$ and the collective velocity of the fluid, $\mathbf{u} = \frac{\sum_i f_i \mathbf{c}_i}{\rho}$). Here, the discrete local equilibria are chosen as a third order Mach-number expansion of the continuum Maxwell-Boltzmann distribution[27]:

$$f_i^{eq} = \rho w_i(1 + \frac{c_{i\lambda}u_\lambda}{c_s^2} + \frac{u_\lambda u_\phi}{2c_s^4}(c_{i\lambda}c_{i\phi} - c_s^2\delta_{\lambda\phi}) + \frac{u_\lambda u_\phi u_\gamma}{6c_s^6}c_{i\gamma}(c_{i\lambda}c_{i\phi} - 3c_s^2\delta_{\lambda\phi})) \tag{2}$$

where $\gamma, \lambda, \phi = x, y, z$ run on spatial dimensions. Equation (1), describes the evolution of the discrete single-particle distribution function in terms of streaming (left hand side) and collision, in the form of a relaxation towards a Maxwellian equilibrium (right hand side), with a characteristic collision frequency ω.

For the sake of clarity, ω is written as the product of two separate factors, one securing compliance with the second laws of thermodynamics (α), the other (β) controlling the kinematic viscosity[28]. More precisely, the kinematic viscosity is given by the following relation:

$$\nu = \frac{c_s^2}{2}(\frac{1}{\beta} - 1) \tag{3}$$

where $c_s = \sqrt{1/3}$ is the lattice speed of sound, α is the largest value of the over-relaxation parameter securing a non decreasing entropy through the relaxation process. The parameter α is determined as the root of the following entropy equality[20,24]:

$$H[f + \alpha(f^{eq} - f)] = H(f) \tag{4}$$

It is straightforward to note that, if $\alpha = 2$, equation (1) reduces to the lattice Boltzmann equation with the Single Relaxation Time (SRT) approximation, so that the entropic scheme is active whenever $\alpha \leq 2$. For further details about the implementation of the entropic correction the readed is referred to[24,29]. The entropic over-relaxation at the liquid-gas interface has proven beneficial for the stabilization of a class of diffuse-interface lattice Boltzmann models based on the discretization of the Korteweg's tensor[15,22,29]. As shown in this work, the same happens with the pseudo-potential approach, where the absence of need for the discretizazion of Korteweg's tensor provides further computational advantages.

Indeed, the entropic estimate acts as a mesoscopic "stabilizer" by locally over-relaxing the collision frequency at the liquid-vapour interface, as we shall comment in more detail in section IV.

The last term in equation (1) accounts for the effect of external/internal forces acting on the fluid molecules and is expressed via the third-order Chapman-Enskog expansion forcing scheme proposed in[16]. This is necessary to identify the errors in the pressure tensor[30], so as to allow an accurate representation of the coexistence curve even at high density ratios, and also to fine-tune the surface tension independently of the equation of state.

In the pseudo-potential scheme, the non-ideal force takes the form[12]:

$$\mathbf{S}(\mathbf{x}, t) = -G\psi(\rho(\mathbf{x}, t))\Delta t \sum_i w_i \mathbf{c}_i \psi(\rho(\mathbf{x} + \mathbf{c}_i \Delta t, t)) \tag{5}$$

where G is the strength of non-ideal interactions and the *generalized density*[14] $\psi(\rho)$ contributes to the excess pressure in the non-ideal equation of state:

$$p = \rho c_s^2 + \frac{G}{2}\psi^2(\rho). \tag{6}$$

In this work, the Peng-Robinson (PR) equation of state (EOS) has been employed, which reads as follows[31]:

$$p = \frac{\rho RT}{1 - b\rho} - \frac{a\Xi\rho^2}{1 + 2b\rho - b^2\rho^2} \tag{7}$$

where $v_T = \sqrt{RT}$ is the thermal speed, a,b are the standard Van der Waals (VdW) parameters associated with the strength of long-range attraction and short-range repulsion and $\Xi = [1 + (0.37464 + 1.54226\zeta - 0.26992\zeta^2)(1 - \sqrt{T/T_c})]^2$, where ζ is the so called acentric factor[31].

The fluid critical temperature and pressure, respectively T_c and p_c, are controlled by the interaction parameters, a and b, and can be easily found via the Maxwell construction[32].

In this work, $a = 0.005$, $b = 0.0952$, $R = 1$ and $\zeta = 0.344$, yielding a critical temperature $T_c = 0.00893$.

Based on Eq.(6), the PR generalized density is computed as:

$$\psi(\rho) = \sqrt{\frac{2}{G}(p - \rho c_s^2)}. \tag{8}$$

where the factor G is inserted only to ensure the positivity of the term under the square root[14].

Moreover, the vapour-liquid viscosity ratio can be tuned by using a variable relaxation time, which reads as follows:

$$\nu = \nu_v + (\nu_l - \nu_g)\frac{\rho - \rho_g}{\rho_l - \rho_g} \tag{9}$$

where ν_v and ν_l are, respectively, the vapour and liquid viscosity. This procedure allows to simulate rheological properties of different gas-liquid mixtures.

A. Wall boundary conditions

The implementation of proper wall boundary conditions is needed to describe the fluid-solid interactions, so as to simulate different wetting properties of the walls[33,34]. Within a pseudo-potential model, this can be achieved by directly imposing the value of the pseudo-potential at the wall nodes. More specifically, it suffices to copy the local bulk values of the pseudo-potential to the wall nodes, with a pre-factor κ_w coding for the intensity of the fluid-solid interaction[35]:

$$\psi(\mathbf{x}_{wall}) = \kappa_w \psi(\mathbf{x}_{fluid}) \tag{10}$$

where $\mathbf{x}_{fluid}$ is the fluid node connected to the wall site, $\mathbf{x}_{wall}$ along the normal direction to the wall. Thus, by setting $\kappa_w < 1$, it is possible to simulate hydrophobic liquid-solid surfaces interactions. As there is still no analytical relation which links κ to the contact angle, it has been set to match the prescribed one.

For the discrete fluid distributions, standard bounce-back conditions have been used to implement no-slip boundary conditions at the wall.

B. The benefits of the entropic formulation

In the following, we discuss the practical benefits of the enhanced stability in actual multiphase flow simulations. All LB simulations require the specification of boundary and initial conditions. The latter are typically chosen sufficiently close to the theoretical equilibrium state, so as to minimize transient effects. With multiphase flows, though, such procedure may eventually fail. Consider a droplet at rest immersed in its vapour, with a large density contrast and strictly zero flow field around. Such steady state is attained through a balance between thermal pressure and surface tension, both taking large but exactly opposite values, thus leading to exact cancellation. Reaching such steady-state starting from initial conditions close to sharp steady-states proves numerically unwieldy because any small unbalance sends out large density waves into the bulk fluid. These waves, in turn, trigger intense recirculation patterns in the vicinity of the frontier, which eventually lead to numerical catastrophe. The standard practice is to start with small/moderate density contrasts and let the system attain the steady-state through a longer sequence of steps, none of which ever involves unsustainable gradients (see figure 2 panel (a)). Of course, this works only within a moderate range of density ratios, typically $30 - 50$ for standard Shan-Chen models. Moreover, this practice naturally leads to the partial coalescence of the vapour phase around the droplet, thus making its size difficult to control during the simulation.

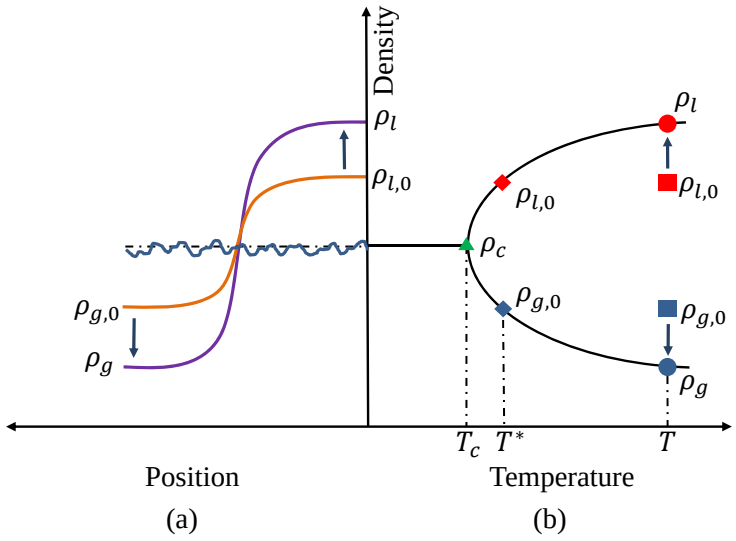

FIG. 2. (a) Sketch of the spinodal curve with the initial density of the liquid droplet ($\rho_{l,0}$) and of the surrounding vapour phase ($\rho_{g,0}$) (square symbol) for a given system temperature T_s, corresponding to an equilibrium thermodynamics state on the same spinodal curve (diamond symbols) for a lower temperature of the system (T^*). The densities of the two phases change in order to reach the steady thermodynamic state (panel (b)), which is represented by the circles on the spinodal curve. During the transient, the vapour phase around the droplet condenses until the droplet diameter complies with the Laplace law. ρ_c i s the mixture density at the critical temperature.

The main benefit of the entropic method is to smooth out the density gradients and damp-down the associated flow fields, thereby allowing to start the simulation from much steeper initial profiles. Like for the case of turbulence, the entropic action is highly localised around the critical regions, in our case the fluid interfaces. The entropic action is represented in figure 3, where we report the *local entropic correction*, defined as $\alpha' = 1 - \alpha/2$, in the initial stage of the simulation of a droplet at rest. The relaxation time is set to $\tau = 0.55$. From this figure it is apparent that α' is localized around the interface and actually never takes up very large values. Nevertheless, such highly-localized, small-amplitude correction is sufficient to tame the fluid instability, which would otherwise ruin a standard pseudo-potential simulation.

III. NUMERICAL RESULTS: VALIDATION

A. Droplet impact on smooth hydrophobic surfaces

As a first test case, we consider the impact of droplets on a hydrophobic surface ($\kappa_w = 0.7 \rightarrow \theta_c = 140°$)[36,37]. A droplet deforms as the result of the impact with a flat solid surface. The main non-dimensional groups, controlling the evolution of the droplet during the impact, are the Weber number ($We = \rho_l U_0^2 D/\sigma$) and the Reynolds number ($Re = U_0 D/\nu$), where U_0 is the speed of the droplet just before the impact with the wall, ρ_l is the density of the droplet, D is the droplet diameter and σ and ν are the surface tension and kinematic viscosity, respectively. The dimensionless deformation, $\frac{D_{max}}{D_0} Re^{-1/5}$, is evaluated for different values of the impact number $P = WeRe^{-4/5}$. For $P < 1$ (capillary regime), the droplet spreading is not limited by the viscous forces and the maximum diameter is found to scale like $D_0 We^{1/4}$. On the contrary, in the viscous regime ($P > 1$), the spreading of the impinging droplet is limited by the effect of the viscosity, with a resulting scaling law of the maximum diameter $D_{max} = D_0 Re^{1/5}$. As one can see from fig. 4, the entropic

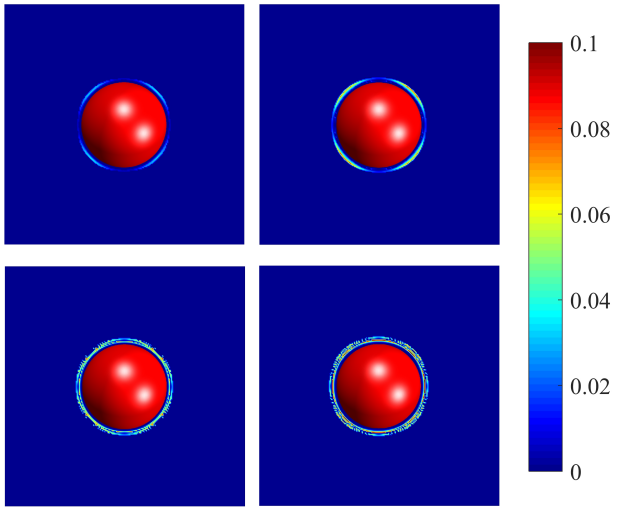

FIG. 3. Local entropic correction field around a static droplet during the initialization stage of the liquid-vapour system. Sequence order is top-left → bottom-right for a total of 200 steps. The entropic halo around the droplet "protects" against numerical instabilities.

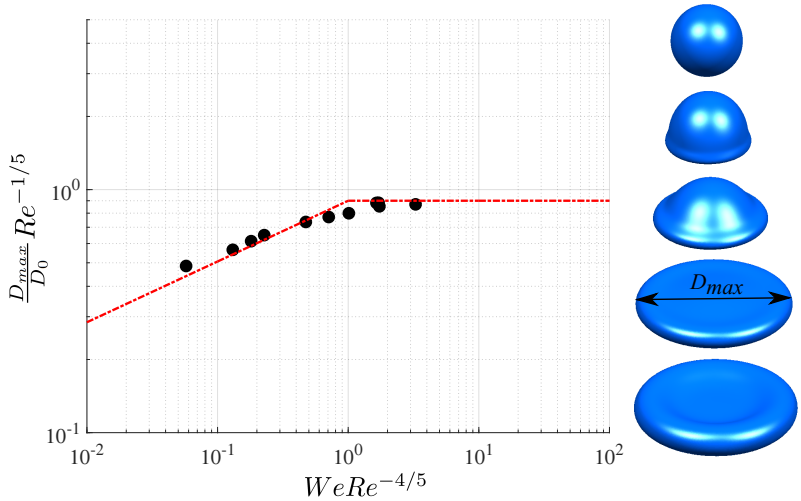

FIG. 4. Dimensionless deformation of an impinging drop (where the maximal extension D_{max} is normalized by the maximal deformation in the viscous regime $D_0 Re^{1/5}$), as a function of the impact number $P = We/Re^{4/5}$. On the right, a typical impact sequence is reported ($We = 85$, $Re = 58$), which is characterized by impact with the wall and formation of the lamella, expansion of the lamella until the maximum radial extension, elastic retraction.

pseudo-potential approach is able to recover the correct deformation of the droplet across a wide range of impact numbers, correctly predicting the transition between the capillary and viscous regime at roughly $P = 1$.

B. Head-on and off-axis droplets collision

Next, we simulate the collision between two droplets of the same diameter. The characteristic non-dimensional groups governing the collision outcome are again the Weber and

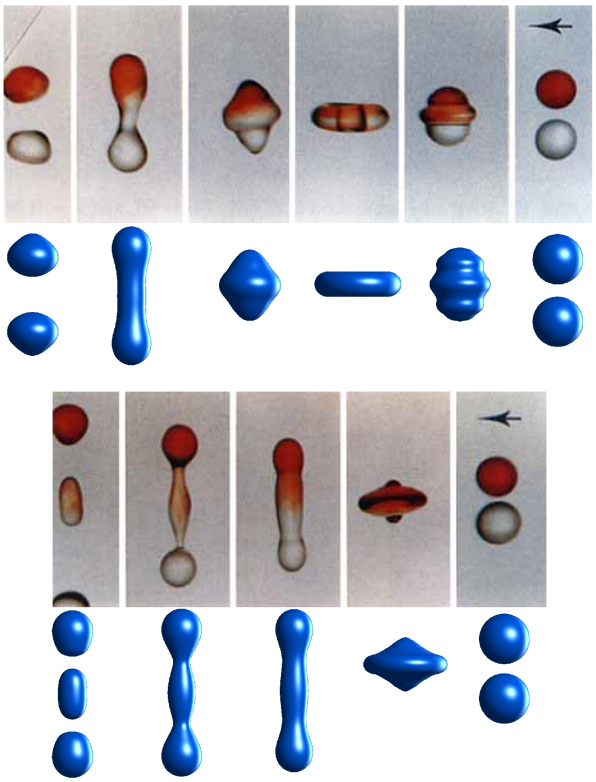

FIG. 5. Head-on droplet collision sequences. The upper and lower panels report different breakup regimes, namely reflexive separation and three-drop reflexive separation, for two different Weber numbers, namely $We \sim 24$ (upper panel) and $We \sim 40$ (lower panel). In both cases, the Reynolds number is set to 1000. The present model is compared against the experimental results of[38].

the Reynolds numbers, now defined as $We = \rho_l U_{rel}^2 D/\sigma$ and $Re = U_{rel} D/\nu$), as well as the impact number, namely the distance between the trajectory lines normalised by the droplet diameter ($b = \chi/D$). We run both head-on and off-axis collisions, comparing the simulation results with the experimental results obtained by[38] (head-on) and[39] (off-axis). As one can see from fig 5, the entropic pseudo-potential results in an excellent agreement with the experimental data of[38], for the head-on droplets collision.

Indeed, it reproduces two different collision outcomes for two different Weber numbers, namely reflexive separation ($Re \sim 1000$ and $We \sim 24$) and reflexive three-droplets separation at $Re \sim 1000$ and $We \sim 41$. These results highlight not only the enhanced stability of the entropic pseudo-potential approach, but also its accuracy, as reflected by the ability to reliably predict different break-up regimes.

We also run off-axis (grazing) droplets collisions, as reported in fig. 6. The numerical results are compared against those of[39], the main parameters, along with the non dimensional numbers of the experiments, being reported in the caption. In this case, the agreement between experimental and numerical results in terms of main features of the interaction between the droplets is again noteworthy, as evidenced by the collision sequence reported in figure 6. Also the end-pinching mechanism of the ligament, described in-depth in[39], is clearly visible and correctly reproduced.

In passing, we note that the current approach permits to access very low viscosities and correspondingly small relaxation times ($\tau < 0.51$), which are beyond reach to previous (non-entropic) pseudo-potential methods. A further inspection of the velocity field figure 7 confirms that the entropic step allows to work with high velocity (up to $\simeq 0.15$), without compromising stability.

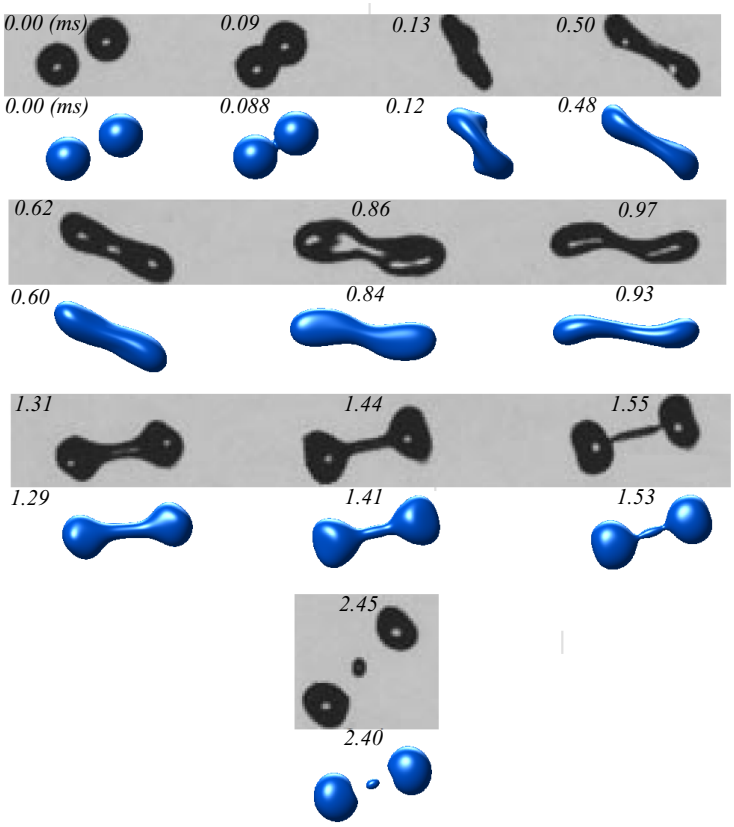

FIG. 6. Collision sequence of off axis droplets collision. The numerical results are compared against the experimental data provided in[39]. The simulation parameters are as follows: impact parameter $b = 0.55$, Weber number $We \sim 60$, Reynolds number $Re \sim 300$. The time step has been computed by employing a dynamical (Reynolds) scaling such that, $\Delta t = \nu_{lb}/\nu_{exp}\Delta x^2$ (ν_{lb} is the numerical viscosity (in lattice unit), ν_{exp} is the physical viscosity (in m^2/s) and Δx is the lattice spacing).

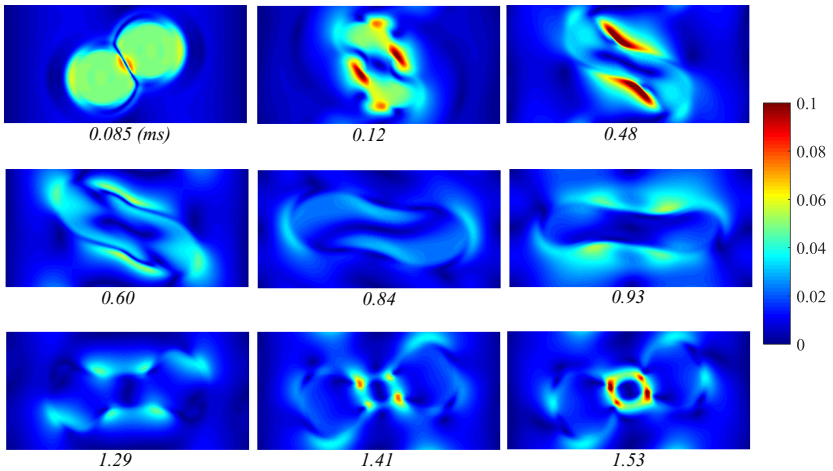

FIG. 7. Snapshots of the velocity field (in $lu/step$) for case $b = 0.55$, Weber number $We \sim 60$, Reynolds number $Re \sim 300$. The stabilization effect of the entropic apporach is demonstrated by the maximum attainable velocity,which can reach $\simeq 0.15$ without spoiling stability (colorbar is limited for visualization purposes).

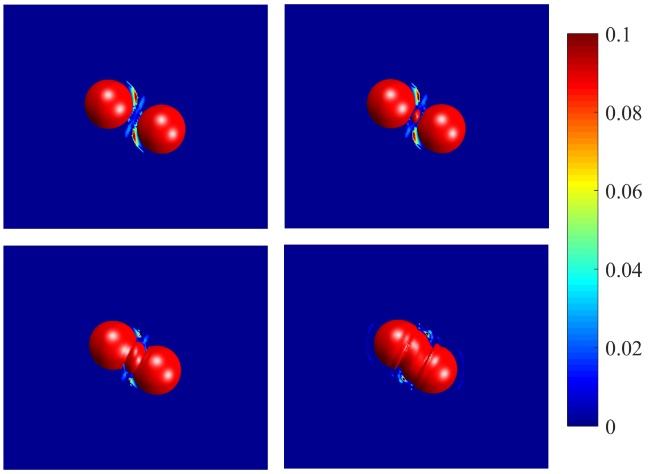

FIG. 8. Local entropic correction field around the two impacting droplets at high Weber and Reynolds numbers. ($We \sim 500, Re \sim 1200$). The Entropy estimate acts as a "fine tuner" of the viscosity around the droplets, where the highest fluid velocities and pressures are met. The figure is a composition of the 3D representation of the droplet, whose color (red) is not to be interpreted according to the color bar, and an equatorial 2d slice of the domain which reports the entropy correction during the impact between the droplets.

IV. NUMERICAL RESULTS: DROPLET COLLISIONS AT HIGH REYNOLDS AND WEBER NUMBERS

In this section, we further demonstrate the stability of the model by performing simulations of droplet off axis collision at $Re \sim 1200$ and $We \sim 500$ and droplet impact on hydrophobic surfaces at $Re \sim 1200$ and $We \sim 200$. At such high We and Re regimes, the pseudo-potential approach would require higher resolutions than the one employed in our simulations.

We run the grazing collisions between two equally sized droplet with an impact parameter $b = 0.55$ at $Re \sim 1200$ and $We \sim 500$. The simulations are performed on a $200 \times 170 \times 170$ lattice. The droplets diameter is $D = 40$ lattice units and the relative velocity between the two droplets is $U_{rel} = 0.2$. The viscosity is set to $\nu = 6.7 \times 10^{-3}$ and the surface tension $\sigma \sim 10^{-3}$, all in lattice units. The density ratio between the liquid and its vapour is about 250.

It is interesting to note that, in a vapour-liquid environment, the collision dynamics is quite rich and complex, presenting some very peculiar phenomena, such as condensation of the interstitial vapour phase, the nucleation of a daughter droplet and its subsequent growth, up to the stage where a merge with the two colliding droplets takes place.

This is documented in fig. 8 which shows: collision of the parent droplets (top left); nucleation of the daughter droplet (top right); growth of the daughter droplet (bottom left); coalescence with the parent droplets (bottom right).

To the best of our knowledge, such phenomenon has never been reported before and will make the subject of further investigation for the future.

Figure 8 shows a sequence of snapshots of the droplet collision. In particular, the local entropic correction is plotted in the xz midplane. From this figure, one appreciates the effect of the entropy estimate, which acts so as to stabilize the SRT model around the droplets and in the interstitial vapour film, where the maximum values of fluid velocity and pressure are met, and locally adjusting the relaxation frequency so as to prevent numerical instabilities.

As a further test, we run the droplet impact on a hydrophobic surface in a high Weber

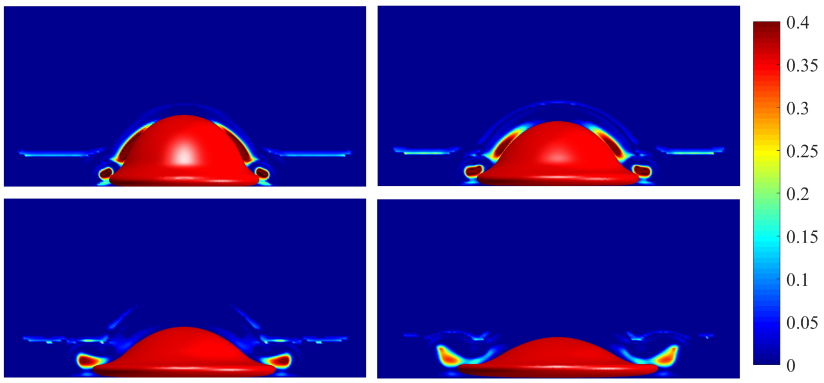

FIG. 9. The local entropic correction around a droplet impinging on a hydrophobic smooth surface. ($Re \sim 1200$, $We \sim 200$). The figure is a composition of the 3D representation of the droplet, whose color (red) is not to be interpreted according to the color bar, and an equatorial 2d slice of the domain which reports the entropy correction during the impact of the droplet with the wall.

and Reynolds number regime. The numerical setup is the same reported in section 4, while the Reynolds and the Weber numbers were set to 1200 and 200, respectively.
In figure 9, the local entropy correction is reported during the most critical stage of the droplet impact, namely, the spreading on the hydrophobic wall. The entropic step locally tunes the relaxation frequency during the spreading stage of the droplet, when the liquid vapour interface moves radially at a very high speed. The entropic stabilizer mainly acts at the tip of the droplet's rim, where the liquid phase pushes radially the surrounding vapour very fast, thus triggering strong fluid recirculations and vortices at the droplet's rim. Even in this case, it is apparent that the entropy correction is localized around the interface. Such highly-localized correction is sufficient to tame the scheme instability, which would otherwise ruin a standard pseudo-potential simulation. It is clear that, in order to correctly simulate the droplet evolution over the entire impact interval, a sufficient number of lattice points is required to discretize both the droplet's rim and the lamella (see[4]). Even with required resolution the plain pseudo-potential approach would not be feasible due to the aforementioned issues related to the initialization difficulties.

V. CONCLUSIONS

Summarizing, we have presented an entropic version of the pseudo-potential lattice Boltzmann method for multiphase flows, and shown that it permits to access Weber and Reynolds numbers regime previously unattainable by standard pseudo-potential methods at comparable resolution. The method has been demonstrated for a variety of complex flows, such as droplet-droplet collisions and droplets impinging on solid walls at Reynolds and Weber numbers up to 1200 and 500, respectively. The present development may offer a new angle of attack to the simulation of complex multiphase flows, such as high-speed droplet-droplet and droplet-wall impacts, with many prospective applications in science and engineering.

REFERENCES

[1] A. B. Kostinski and R. A. Shaw, "Droplet dynamics: Raindrops large and small," Nature Physics **5**, 624–625 (2009).
[2] Z. Yoshimitsu, A. Nakajima, T. Watanabe, and K. Hashimoto, "Effects of surface structure on the hydrophobicity and sliding behavior of water droplets," Langmuir **18**, 5818–5822 (2002).

[3]S. Moon, S. K. Hasan, Y. S. Song, F. Xu, H. O. Keles, F. Manzur, S. Mikkilineni, J. W. Hong, J. Nagatomi, E. Haeggstrom, *et al.*, "Layer by layer three-dimensional tissue epitaxy by cell-laden hydrogel droplets," Tissue Engineering Part C: Methods **16**, 157–166 (2009).

[4]C. W. Visser, P. E. Frommhold, S. Wildeman, R. Mettin, D. Lohse, and C. Sun, "Dynamics of high-speed micro-drop impact: numerical simulations and experiments at frame-to-frame times below 100 ns," Soft Matter **11**, 1708–1722 (2015).

[5]S. Lin and R. Reitz, "Drop and spray formation from a liquid jet," Annual Review of Fluid Mechanics **30**, 85–105 (1998).

[6]D. M. Anderson, G. B. McFadden, and A. A. Wheeler, "Diffuse-interface methods in fluid mechanics," Annual review of fluid mechanics **30**, 139–165 (1998).

[7]R. Scardovelli and S. Zaleski, "Direct numerical simulation of free-surface and interfacial flow," Annual review of fluid mechanics **31**, 567–603 (1999).

[8]S. Succi, "Lattice boltzmann across scales: from turbulence to dna translocation," The European Physical Journal B-Condensed Matter and Complex Systems **64**, 471–479 (2008).

[9]S. Succi, "Lattice boltzmann 2038," EPL (Europhysics Letters) **109**, 50001 (2015).

[10]A. Montessori, P. Prestininzi, M. La Rocca, and S. Succi, "Lattice boltzmann approach for complex nonequilibrium flows," Physical Review E **92**, 043308 (2015).

[11]A. Montessori, P. Prestininzi, M. La Rocca, G. Falcucci, S. Succi, and E. Kaxiras, "Effects of knudsen diffusivity on the effective reactivity of nanoporous catalyst media," Journal of Computational Science **17**, 377–383 (2016).

[12]X. Shan and H. Chen, "Lattice boltzmann model for simulating flows with multiple phases and components," Physical Review E **47**, 1815 (1993).

[13]A. Montessori, G. Falcucci, M. La Rocca, S. Ansumali, and S. Succi, "Three-dimensional lattice pseudopotentials for multiphase flow simulations at high density ratios," Journal of Statistical Physics **161**, 1404–1419 (2015).

[14]P. Yuan and L. Schaefer, "Equations of state in a lattice boltzmann model," Physics of Fluids **18**, 042101 (2006).

[15]S. Chikatamarla, I. Karlin, *et al.*, "Entropic lattice boltzmann method for multiphase flows," Physical review letters **114**, 174502 (2015).

[16]D. Lycett-Brown and K. H. Luo, "Improved forcing scheme in pseudopotential lattice boltzmann methods for multiphase flow at arbitrarily high density ratios," Physical Review E **91**, 023305 (2015).

[17]R. Benzi, M. Sbragaglia, S. Succi, M. Bernaschi, and S. Chibbaro, "Mesoscopic lattice boltzmann modeling of soft-glassy systems: theory and simulations," The Journal of Chemical Physics **131**, 104903 (2009).

[18]G. Falcucci, G. Bella, G. Chiatti, S. Chibbaro, M. Sbragaglia, and S. Succi, "Lattice boltzmann models with mid-range interactions," Communications in computational physics **2**, 1071–1084 (2007).

[19]M. Sega, M. Sbragaglia, S. S. Kantorovich, and A. O. Ivanov, "Mesoscale structures at complex fluid–fluid interfaces: a novel lattice boltzmann/molecular dynamics coupling," Soft Matter **9**, 10092–10107 (2013).

[20]S. Ansumali and I. V. Karlin, "Single relaxation time model for entropic lattice boltzmann methods," Physical Review E **65**, 056312 (2002).

[21]F. Bösch, S. S. Chikatamarla, and I. V. Karlin, "Entropic multirelaxation lattice boltzmann models for turbulent flows," Physical Review E **92**, 043309 (2015).

[22]A. Mazloomi, S. S. Chikatamarla, and I. V. Karlin, "Entropic lattice boltzmann method for multiphase flows: Fluid-solid interfaces," Physical Review E **92**, 023308 (2015).

[23]B. Dorschner, S. Chikatamarla, and I. Karlin, "Transitional flows with the entropic lattice boltzmann method," Journal of Fluid Mechanics **824**, 388–412 (2017).

[24]I. Karlin, A. Ferrante, and H. Öttinger, "Perfect entropy functions of the lattice boltzmann method," EPL (Europhysics Letters) **47**, 182 (1999).

[25]R. Benzi, S. Succi, and M. Vergassola, "The lattice boltzmann equation: theory and applications," Physics Reports **222**, 145–197 (1992).

[26]S. Ansumali, I. V. Karlin, and H. C. Öttinger, "Minimal entropic kinetic models for hydrodynamics," EPL (Europhysics Letters) **63**, 798 (2003).

[27]X. Shan, X.-F. Yuan, and H. Chen, "Kinetic theory representation of hydrodynamics: a way beyond the navier-stokes equation," Journal of Fluid Mechanics **550**, 413 (2006).

[28]B. Dorschner, F. Bösch, S. Chikatamarla, K. Boulouchos, and I. Karlin, "Entropic multi-relaxation time lattice boltzmann model for complex flows," Journal of Fluid Mechanics **801**, 623–651 (2016).

[29]A. M. Moqaddam, S. S. Chikatamarla, and I. V. Karlin, "Simulation of binary droplet collisions with the entropic lattice boltzmann method," Physics of Fluids (1994-present) **28**, 022106 (2016).

[30]M. Sbragaglia and D. Belardinelli, "Interaction pressure tensor for a class of multicomponent lattice boltzmann models," Physical Review E **88**, 013306 (2013).

[31]D.-Y. Peng and D. B. Robinson, "A new two-constant equation of state," Industrial & Engineering Chemistry Fundamentals **15**, 59–64 (1976).

[32]J. Clerk-Maxwell, "On the dynamical evidence of the molecular constitution of bodies," Nature **11**, 357–359 (1875).

[33]R. Benzi, L. Biferale, M. Sbragaglia, S. Succi, and F. Toschi, "Mesoscopic modeling of a two-phase flow in the presence of boundaries: the contact angle," Physical Review E **74**, 021509 (2006).

[34]N. S. Martys and H. Chen, "Simulation of multicomponent fluids in complex three-dimensional geometries by the lattice boltzmann method," Phys. Rev. E **53**, 743–750 (1996).

[35]A. De Maio, S. Palpacelli, and S. Succi, "A new boundary condition for three-dimensional lattice boltzmann simulations of capillary filling in rough micro-channels," Communications in Computational Physics **9**, 1284–1292 (2011).

[36]D. Richard, C. Clanet, and D. Quéré, "Surface phenomena: Contact time of a bouncing drop," Nature **417**, 811–811 (2002).

[37]C. Clanet, C. Béguin, D. Richard, and D. Quéré, "Maximal deformation of an impacting drop," Journal of Fluid Mechanics **517**, 199–208 (2004).

[38]N. Ashgriz and J. Poo, "Coalescence and separation in binary collisions of liquid drops," Journal of Fluid Mechanics **221**, 183–204 (1990).

[39]J. Qian and C. Law, "Regimes of coalescence and separation in droplet collision," Journal of Fluid Mechanics **331**, 59–80 (1997).